

# Real-time detection reveals that effectors couple dynamin's GTP-dependent conformational changes to the membrane

Rajesh Ramachandran and Sandra L Schmid\*

Department of Cell Biology, The Scripps Research Institute, La Jolla, CA, USA

The GTPase dynamin is a mechanochemical enzyme involved in membrane fission, but the molecular nature of its membrane interactions and their regulation by guanine nucleotides and protein effectors remain poorly characterized. Using site-directed fluorescence labeling and several independent fluorescence spectroscopic techniques, we have developed robust assays for the detection and real-time monitoring of dynamin–membrane and dynamin–dynamin interactions. We show that dynamin interacts preferentially with highly curved, PIP<sub>2</sub>-dense membranes and inserts partially into the lipid bilayer. Our kinetic measurements further reveal that cycles of GTP binding and hydrolysis elicit major conformational rearrangements in self-assembled dynamin that favor dynamin–membrane association and dissociation, respectively. Sorting nexin 9, an abundant dynamin partner, transiently stabilizes dynamin on the membrane at the onset of stimulated GTP hydrolysis and may function to couple dynamin's mechanochemical conformational changes to membrane destabilization. Amphiphysin I has the opposite effect. Thus, dynamin's mechanochemical properties on a membrane surface are dynamically regulated by its GTPase cycle and major binding partners.

*The EMBO Journal* (2008) 27, 27–37. doi:10.1038/sj.emboj.7601961; Published online 13 December 2007  
**Subject Categories:** membranes & transport; proteins  
**Keywords:** conformational changes; dynamin; effectors; fluorescence spectroscopy; membrane fission

## Introduction

During the terminal stages of endocytic clathrin-coated vesicle formation, the large GTPase dynamin self-assembles into collar-like structures around the necks of deeply invaginated coated pits and catalyzes vesicle scission by mechanisms that remain poorly characterized (for reviews, see Hinshaw, 2000; Conner and Schmid, 2003). This modular GTPase (Figure 1A) is initially recruited to nascent coated pits via interactions between its C-terminal proline/arginine-rich domain (PRD)

and Src homology 3 (SH3) domain-containing binding partners (Shpetner *et al*, 1996; Okamoto *et al*, 1997). Subsequent interactions mediated by its pleckstrin homology (PH) domain with phosphatidylinositol-4,5-bisphosphate (PIP<sub>2</sub>) at the membrane surface are, however, required for its *in vivo* function (Achiriloaie *et al*, 1999; Lee *et al*, 1999; Vallis *et al*, 1999). The middle domain and GTPase effector domain (GED) are both involved in self-assembly, and the latter is involved also in the stimulation of assembly-dependent GTPase activity (Sever *et al*, 1999; Song *et al*, 2004; Ramachandran *et al*, 2007).

Dynamin self-assembles spontaneously into rings and helical spirals onto negatively charged phospholipid-containing liposomes and lipid nanotubes to form protein-encircled lipid tubules that resemble the collared necks observed *in vivo* (Sweitzer and Hinshaw, 1998; Stowell *et al*, 1999). EM observations have revealed distinct conformational changes in self-assembled dynamin that result either in the constriction of dynamin spirals on liposomes upon GTP binding (Zhang and Hinshaw, 2001; Chen *et al*, 2004; Danino *et al*, 2004) or an increase in pitch and corresponding elongation of the spirals on preformed lipid nanotubes upon GTP hydrolysis (Stowell *et al*, 1999). Whether the distinct conformational changes detected in these static images reflect differences in experimental conditions (membrane templates, dynamin concentration, etc.) or distinct template-stabilized stages of the dynamin GTPase cycle remains to be determined. More recent light microscopy studies have suggested that a GTPase-driven twisting rotation of assembled dynamin around the underlying membrane tubule mediates fission (Roux *et al*, 2006). Although these studies provide important clues into the global conformational changes in self-assembled dynamin during its GTP hydrolysis cycle, they offer very little insight into either the molecular nature or the dynamics of dynamin's interactions with the membrane and also with itself.

To further elucidate the nature of these interactions and their dynamics, and to gain new insight into the mechanisms underlying membrane fission, we have developed fluorescence spectroscopic assays to measure dynamin–membrane and dynamin–dynamin interactions in real time and used these to identify the role of nucleotide-dependent conformational changes and effectors in regulating dynamin's mechanochemical activities at the membrane.

## Results

### **A real-time assay for dynamin–membrane interactions**

Fluorescence spectroscopy coupled to the site-specific fluorescence labeling of proteins is a powerful approach for determining protein interactions, conformations and mechanisms that occur at a membrane surface (Ramachandran *et al*, 2004, 2005; Johnson, 2005). Quantifiable data can be

\*Corresponding author. Department of Cell Biology, The Scripps Research Institute, 10550 N. Torrey Pines Road, La Jolla, CA 92037, USA. Tel.: +1 858 784 2311; Fax: +1 858 784 2345; E-mail: slschmid@scripps.edu

Received: 8 August 2007; accepted: 21 November 2007; published online: 13 December 2007

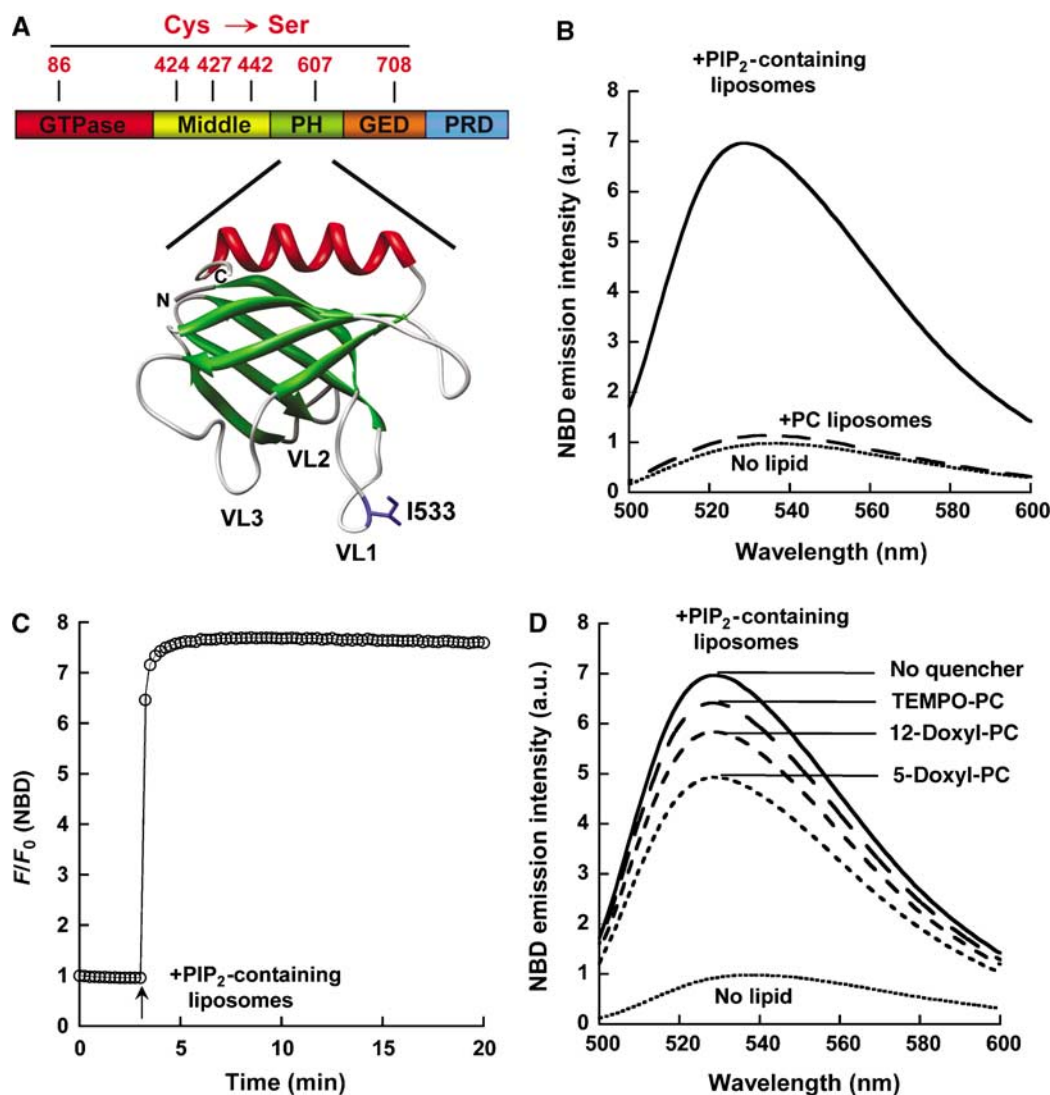


**Figure 1** A fluorescence-based assay for dynamin–membrane interactions. (A) Schematic illustration of dynamin domain arrangement and ribbon representation of the human dynamin 1 PH domain crystal structure (PDB ID: 1dyn). GED, GTPase effector domain; PH, pleckstrin homology; PRD, proline and arginine-rich domain. Positions of the Cys residues replaced with Ser are indicated and variable loops 1–3 (VL1–3) in the PH domain are labeled. The location of I533 in VL1 that was replaced with a Cys (I533C) in this study is shown in stick representation. (B) Representative NBD emission spectra for 0.5 μM NBD-dynamin before and after incubation with either 15 mol% PIP<sub>2</sub>-containing liposomes or 100 mol% DOPC liposomes (150 μM total lipid). (C) Time-dependent emission intensity profile for 0.1 μM NBD-dynamin before and after addition of 15 mol% PIP<sub>2</sub>-containing liposomes (30 μM total lipid). For this and all subsequent figures, unless otherwise stated,  $F_0$  is the initial intensity of NBD-dynamin before addition of lipid (at time = 0) and  $F$  is the intensity at time  $t$ . Representative data from at least three independent experiments are indicated as  $F/F_0$  and plotted versus time. (D) Quenching of NBD fluorescence by nitroxide moieties located at different depths in the membrane bilayer. Representative NBD emission spectra for 0.5 μM NBD-dynamin before and after incubation with either 15 mol% PIP<sub>2</sub>-containing liposomes (no quencher) or with 15 mol% PIP<sub>2</sub>-containing liposomes that also contain 10 mol% of the indicated nitroxide-labeled phospholipid (150 μM total lipid).

obtained from very low concentrations of fluorescently labeled protein, as can information regarding probe environment, intermolecular proximity, etc. Furthermore, changes in the fluorescence signal can be monitored as a function of time to obtain kinetic information on conformational changes not possible with EM, X-ray crystallography or other related techniques. Therefore, to study the dynamics of dynamin–membrane and dynamin–dynamin interactions, we developed fluorescence-based assays and used low protein concentrations (typically  $\leq 0.1 \mu\text{M}$ ) that would permit the formation of only physiologically relevant short dynamin assemblies on model liposomal membranes.

For the site-specific labeling, we engineered a functional derivative of human dynamin-1 (Figure 1A) in which six of

the seven native Cys residues (at positions 86, 424, 427, 442, 607 and 708) were substituted with Ser, hereafter referred to as reactive-Cys-less dynamin or RCL-Dyn. This derivative, containing a critical, partially buried native Cys at residue 169 in the GTPase domain, was largely unreactive to thiol-modifying reagents under our labeling conditions (data not shown).

The PH domain of dynamin (Figure 1A) is responsible for PIP<sub>2</sub> headgroup recognition and membrane binding (Salim *et al*, 1996; Vallis *et al*, 1999). The key residues involved in this association reside in the variable loops (VL1–3; Figure 1A) (Salim *et al*, 1996; Zheng *et al*, 1996), and mutation of a critical Lys residue (K535A) in VL1 abrogates membrane binding (Vallis *et al*, 1999). Therefore, to detect

**Table I** Quenching of NBD-dynamamin emission by quenchers located at different depths in the membrane bilayer

| State        | $F_{\text{TEMPO-PC}}/F_{\text{no quencher}}$ | $F_{5\text{-doxyl-PC}}/F_{\text{no quencher}}$ | $F_{12\text{-doxyl-PC}}/F_{\text{no quencher}}$ |
|--------------|--|--|---|
| – Nucleotide | $0.91 \pm 0.02$                              | $0.70 \pm 0.01$                                | $0.83 \pm 0.01$                                 |
| + GMPPCP     | $0.84 \pm 0.04$                              | $0.65 \pm 0.01$                                | $0.79 \pm 0.04$                                 |

Experiments were done as indicated in Figure 1D. NBD was excited at 470 nm and emission measured at 530 nm.  $F_{\text{no quencher}}$ ,  $F_{\text{TEMPO-PC}}$ ,  $F_{5\text{-doxyl-PC}}$  and  $F_{12\text{-doxyl-PC}}$  each represent  $F/F_0$  values obtained for NBD-dynamamin incubated with 15 mol% PIP<sub>2</sub>-containing liposomes that either lack (no quencher) or contain 10 mol% of either TEMPO-PC, 5-doxyl-PC, or 12-doxyl-PC, respectively.  $F_0$  and  $F$  are the emission-intensity values observed for NBD-dynamamin before and after incubation with the corresponding liposomes, respectively. The values shown are the average of ratios  $\pm$  s.d. determined from at least three independent experiments.

dynamamin–membrane interactions, we introduced a single reactive Cys residue in VL1 of the PH domain by replacing Ile at position 533 (RCL-Dyn<sup>I533C</sup>). I533 is not conserved between dynamamin-1 and dynamamin-2 isoforms. This Cys was covalently modified with the environment-sensitive fluorophore NBD, to yield RCL-Dyn<sup>I533C-NBD</sup> (hereafter referred to as NBD-dynamamin). It has previously been reported that the isoform specificity of I533 and the post-translational nitrosylation of C607 play important roles for dynamamin 1 functions *in vivo* (Artalejo *et al*, 1997; Wang *et al*, 2006); and, indeed, we find that overexpression of RCL-Dyn<sup>I533C</sup> in tTA-HeLa cells inhibited transferrin uptake (data not shown). However, we were unable to detect any defect in the *in vitro* activities of this mutant dynamamin or its NBD-labeled derivative, including either lipid-binding ability or assembly-stimulated and basal GTPase activities, each of which were indistinguishable from those of WT-dynamamin (Supplementary Figure 1A–C). As neither the multiple mutations nor the fluorophore conjugation affected the enzymatic or assembly properties of dynamamin, this modified dynamamin serves as a valid tool for probing the mechanochemical coupling of these activities *in vitro*.

Movement of NBD from an aqueous milieu to a nonpolar environment such as the hydrocarbon core of a membrane bilayer is accompanied by a pronounced increase in emission intensity (Ramachandran *et al*, 2002). Indeed, when NBD-dynamamin was incubated with 15 mol% PIP<sub>2</sub>-containing liposomes at concentrations that allowed near-complete binding of dynamamin to membranes (protein-to-lipid molar ratio of 1:300), a dramatic six- to eightfold increase in NBD emission intensity was observed (Figure 1B). The change in NBD emission intensity could be monitored in real time upon addition of target membranes, thereby providing a sensitive assay for determining the kinetics of these interactions (Figure 1C) that was not possible previously by sedimentation.

Control experiments established the validity of this assay. First, in the presence of pure phosphatidylcholine (PC) liposomes that do not detectably bind dynamamin, only a negligible increase in NBD emission intensity was observed (Figure 1B). Second, no change in NBD emission intensity was detected when the NBD moiety was conjugated to a Cys residue introduced in the GTPase domain, RCL-Dyn<sup>S306C-NBD</sup> (Supplementary Figure 2), establishing that the assay detected direct PH domain–membrane interactions.

#### Dynamamin inserts partially into the lipid bilayer

To determine the nature of dynamamin–membrane interactions, we measured the accessibility of the NBD fluorophore to membrane-restricted collisional quenching agents, here un-

charged nitroxide moieties attached either to the acyl chain or the headgroup of phospholipid molecules (Figure 1D). By comparing the extents of quenching from nitroxide moieties localized at different depths within the membrane bilayer, the relative membrane penetration depth of the dye can be determined (Shatursky *et al*, 1999; Ramachandran *et al*, 2002). Collisional quenching was observed from nitroxide moieties attached to the phospholipid headgroup (TEMPO-PC), the 5th (5-doxyl-PC) and the 12th (12-doxyl-PC) carbon positions of the phospholipid acyl chain, confirming that the increase in NBD emission intensity reflects dynamamin–membrane association. The extent of quenching from these positions varied significantly with 5-doxyl-PC > 12-doxyl-PC > TEMPO-PC (Figure 1D, Table I), indicating a shallow disposition of the PH domain VL1 within the acyl chain region of the lipid bilayer. In the presence of the non-hydrolyzable GTP analog, GMPPCP, no change in the pattern of quenching, and therefore the insertion depth of the PH domain, was observed (Table I). However, the marginal increase in the extents of quenching from all quencher positions (Table I) suggests that GTP binding induces a conformational rearrangement in dynamamin that increases the relative accessibility of the NBD dyes to the nitroxide moieties.

#### Dynamamin–membrane association is highly dependent on PIP<sub>2</sub> spatial density

Using this quantitative assay, we next determined the affinity of NBD-dynamamin for PIP<sub>2</sub>-containing liposomes. The apparent binding affinity was >10-fold higher when PIP<sub>2</sub> was present at 15 mol% ( $K_D = 1.9 \pm 0.3 \mu\text{M}$ ) versus 2 mol% ( $K_D(\text{app}) > 15 \mu\text{M}$ ) of the total lipid present (Figure 2A). When dynamamin–membrane association was measured at a fixed total lipid concentration while the mol% of PIP<sub>2</sub> per liposome was varied, we obtained a sigmoidal binding isotherm indicating that dynamamin binding is cooperative with respect to local PIP<sub>2</sub> concentration (Hill constant,  $n_H = 2.8 \pm 0.3$ ; goodness of fit  $R^2 > 0.99$ ) (Figure 2B). The much reduced association of NBD-dynamamin with 2 mol% PIP<sub>2</sub>- versus 15 mol% PIP<sub>2</sub>-containing liposomes also occurred at a slower rate and exhibited biphasic kinetics (Figure 2C), presumably corresponding to an initial fast association with a preexisting fraction of clustered PIP<sub>2</sub> followed by a slow rate of binding to diffuse PIP<sub>2</sub> molecules that are eventually clustered through dynamamin polymerization. This slow second phase was not observed with 15 mol% PIP<sub>2</sub>-containing liposomes (Figure 2C, inset). Collectively, these data establish that dynamamin tetramers preferentially bind to and self-assemble on membranes bearing a high spatial density of PIP<sub>2</sub>.

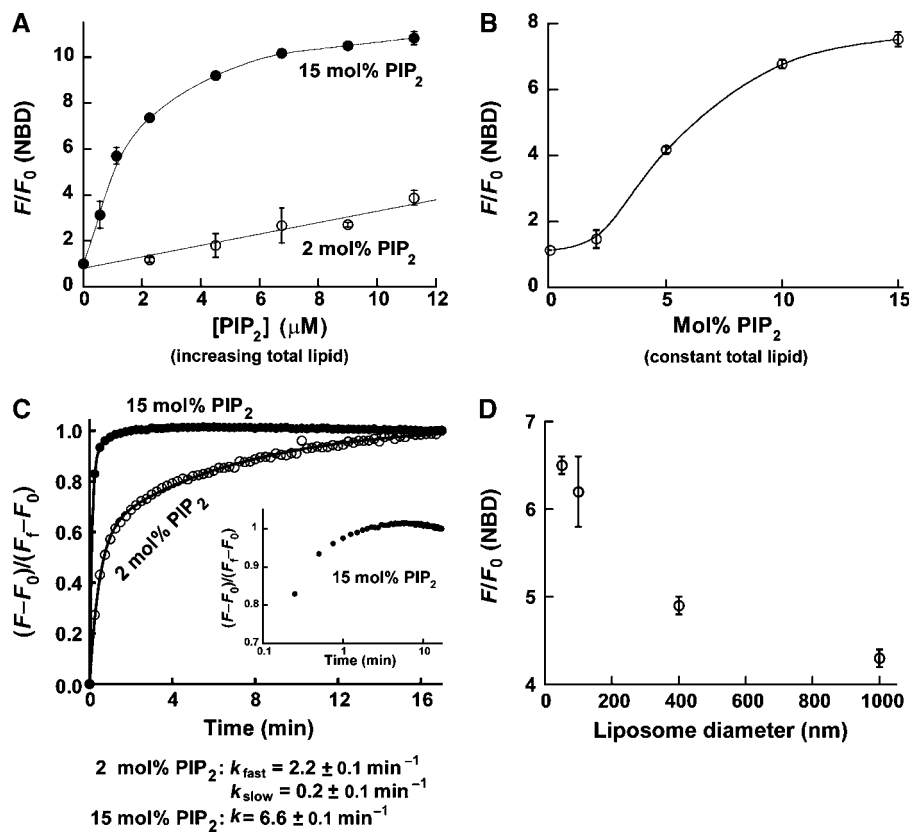


**Figure 2** Dynamin–membrane interaction is highly sensitive to  $PIP_2$  spatial density and membrane curvature. (A) Binding of  $0.1 \mu M$  NBD-dynamin to increasing concentration of liposomes containing either 2 mol% ( $\circ$ ) or 15 mol% ( $\bullet$ )  $PIP_2$ . The average membrane-dependent intensity increase is indicated as  $F/F_0$ . (B) Binding of  $0.1 \mu M$  NBD-dynamin to a fixed concentration of liposomes ( $30 \mu M$  total lipid) with increasing content of  $PIP_2$  (0–15 mol%). (C) Normalized time-dependent NBD emission intensity profiles for  $0.1 \mu M$  NBD-dynamin upon addition of either 2 mol% ( $\circ$ ) or 15 mol% ( $\bullet$ )  $PIP_2$ -containing liposomes ( $30 \mu M$  total lipid). To allow direct comparison of the rate of change of NBD fluorescence, each intensity profile was normalized to  $F_f$ , the final intensity at  $t = 17$  min after liposome addition, and plotted as the total fractional intensity change as a function of time. Data were best fit to either a one-phase (for 15 mol%  $PIP_2$ ) or a two-phase (for 2 mol%  $PIP_2$ ) association model as described in Supplementary data to obtain the indicated rate constants. (Inset) Binding of NBD-dynamin to 15 mol%  $PIP_2$ -containing liposomes is plotted against the log of time in minutes. (D) Binding of  $0.1 \mu M$  NBD-dynamin to 15 mol%  $PIP_2$ -containing liposomes ( $30 \mu M$  total lipid) of varying diameter. The average membrane-dependent intensity increase of three independent experiments is indicated as  $F/F_0$ .

### Dynamin–membrane association is sensitive to membrane curvature

Large dynamic changes in membrane curvature at the coated pit precede clathrin-coated vesicle formation at the plasma membrane (Conner and Schmid, 2003; McMahon and Gallop, 2005). To determine the sensitivity of dynamin–membrane interactions to membrane curvature, we examined the binding of NBD-dynamin to  $PIP_2$ -containing liposomes ranging between 50 nm and  $1 \mu m$  in diameter, representing a gradual decrease in membrane curvature. Dynamin binding increased with decreasing liposome diameter, indicating a higher affinity for more highly curved membranes (Figure 2D).

### Guanine nucleotides regulate dynamin–membrane interactions

The time resolution of our fluorescence-based assay next allowed us to investigate the effect of guanine nucleotides on dynamin–membrane interactions. Addition of GMPPCP to NBD-dynamin first bound saturably to  $PIP_2$ -containing liposomes in the absence of nucleotides did not elicit any appreciable change in emission intensity, indicating that GTP binding does not increase or alter dynamin–membrane association (Figure 3A). In contrast, addition of GDP elicited

the rapid dissociation of dynamin, suggesting that, in its GDP-bound state, dynamin adopts a conformation that significantly weakens its interaction with the membrane (Figure 3A), resulting in an altered equilibrium distribution between membrane-associated and free dynamin. Unexpectedly, addition of GTP also triggered rapid dynamin dissociation (Figure 3A). This rapid decrease in membrane association was not a consequence of the total conversion of GTP to GDP, as  $<5\%$  of the total GTP was consumed during this time course (Supplementary Figure 1D). Moreover, similar results were obtained in the presence of a GTP regenerating system (Supplementary Figures 3A and B). Together, these data suggest that rapid GTP hydrolysis by membrane-associated, self-assembled dynamin is accompanied by dynamin release from the membrane, reaching a new steady state that reflects cycles of membrane association and dissociation during GTP binding and hydrolysis, respectively. Stimulated GTP hydrolysis reproducibly triggered dynamin dissociation at a faster rate and to a slightly larger extent than GDP ( $k_{GTP} = 2.2 \pm 0.1 \text{ min}^{-1} > k_{GDP} = 1.6 \pm 0.1 \text{ min}^{-1}$ ) (Figure 3A). This difference likely reflects the reported 40-fold-greater GTP binding affinity of dynamin (Binns *et al*, 1999) and the expected higher GDP occupancy in the active

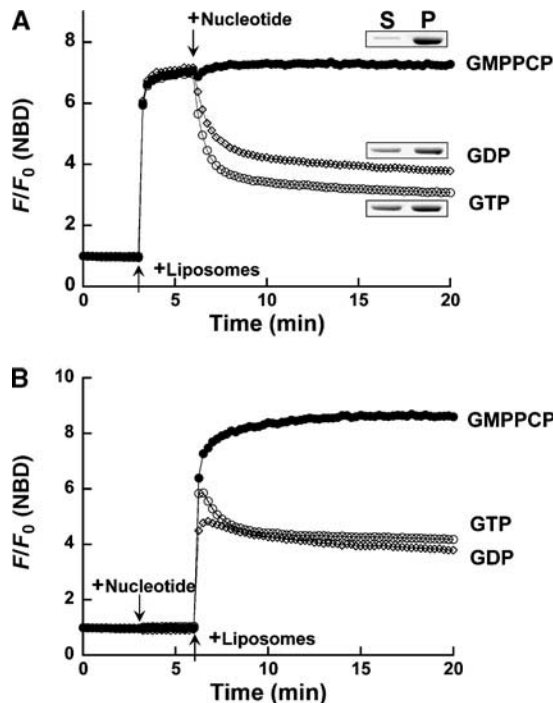


**Figure 3** Guanine nucleotides regulate dynamin–membrane interactions. (A) Representative time-dependent emission-intensity profiles for 0.1  $\mu\text{M}$  NBD-dynamin before and after sequential additions (see arrows) of 15 mol%  $\text{PIP}_2$ -containing liposomes (30  $\mu\text{M}$  total lipid) at 3 min and the indicated nucleotides (1 mM final) at 6 min; GMPPCP ( $\bullet$ ), GDP ( $\diamond$ ), GTP ( $\circ$ ). (Insets) Sedimentation analysis of 0.5  $\mu\text{M}$  NBD-dynamin after incubation for 20 min at 25°C with 15 mol%  $\text{PIP}_2$ -containing liposomes (150  $\mu\text{M}$  total lipid) and the indicated nucleotide (1 mM final) was performed as described under Methods. The supernatant (S) and pellet (P) fractions were subjected to SDS–PAGE and visualized by Coomassie blue staining. See Supplementary Figure 3C for quantification of data from three independent experiments. (B) Representative time-dependent emission-intensity profiles for 0.1  $\mu\text{M}$  NBD-dynamin were acquired as in (A) except that the indicated nucleotides (1 mM final) now were added before (at 3 min) the addition of  $\text{PIP}_2$ -containing liposomes.

sites after it is generated locally from high-affinity GTP binding and hydrolysis rather than from low-affinity binding of GDP directly from solution. Sedimentation analyses at steady state confirmed that the NBD emission decrease observed upon addition of either GTP or GDP was due to dynamin–membrane dissociation and not to a nucleotide-dependent conformational change in membrane-bound dynamin that repositions NBD relative to the bilayer core (Figure 3A, insets; Supplementary Figure 3C).

Similar results were obtained when liposomes were added to dynamin in the presence of various nucleotides (Figure 3B). Dynamin bound rapidly to liposomes in the presence of GMPPCP and reached saturation at the same level as in the absence of nucleotides. The presence of GDP drastically reduced dynamin–membrane association (40% of the steady-state intensity obtained with GMPPCP). In the presence of GTP, addition of  $\text{PIP}_2$ -containing liposomes to NBD-dynamin resulted in a transient burst of NBD emission intensity increase followed by a relatively slow decrease at the onset of stimulated GTP hydrolysis to reach steady state comparable to that observed in the presence of GDP (Figure 3B). Collectively, these data indicate that in its

GMPPCP- or GTP-bound state, dynamin exhibits a higher affinity for  $\text{PIP}_2$ -containing membranes than in the GDP-bound state, but that GTP hydrolysis rapidly destabilizes dynamin–membrane interactions.

### GTP hydrolysis drives a major conformational rearrangement in dynamin

How might dynamin trigger membrane fission if, under physiological conditions of GTP binding and hydrolysis, it rapidly dissociates from membranes? To address this question, we sought evidence for nucleotide-dependent conformational changes in self-assembled dynamin. To this end, we developed an assay that directly monitors dynamin–dynamin interactions in real time (Ramachandran *et al*, 2007) using WT-dynamin surface labeled with the thiol-reactive derivative of the fluorophore BODIPY-F1 (hereafter referred to as BODIPY-dynamin). Like NBD-dynamin, the basal and assembly-stimulated GTPase activities of BODIPY-dynamin, as well as its ability to bind liposomes, were indistinguishable from those of WT-dynamin (Supplementary Figure 1A–C). The close proximity of BODIPY fluorophores upon BODIPY-dynamin self-assembly leads to fluorescence self-quenching (see Methods) and provides a direct measure of dynamin–dynamin interactions.

Addition of  $\text{PIP}_2$ -containing liposomes to BODIPY-dynamin elicited a rapid, saturable decrease in emission intensity, indicating dynamin self-assembly onto the membrane surface (Figure 4A). Consistent with this interpretation, the kinetics of BODIPY-dynamin self-assembly were nearly superimposable with that of NBD-dynamin–membrane association (Supplementary Figure 4). Moreover, in control experiments with the lipid binding-defective, BODIPY-labeled Dyn1-K535A mutant (Figure 4B), or with an assembly-defective Dyn1 mutant (Ramachandran *et al*, 2007), no significant change in BODIPY emission intensity was observed. These data also provide further evidence that the lipid-binding and assembly properties of the differentially labeled dynamin derivatives (BODIPY-dynamin versus NBD-dynamin) are comparable and together demonstrate that dynamin membrane binding and self-assembly are tightly coupled.

We next used this assay to determine the effects of guanine nucleotides on dynamin self-assembly. Addition of GMPPCP to self-assembled dynamin resulted in the further quenching of BODIPY emission until a new steady state was obtained (Figure 4A). Because no corresponding change in NBD emission intensity was observed under identical conditions (Figure 3A), we interpret this BODIPY emission intensity change to reflect a GMPPCP-dependent conformational rearrangement in self-assembled dynamin that brings adjacent BODIPY fluorophores into closer proximity. Conversely, addition of GDP resulted in the dequenching of BODIPY emission, indicating a slow rate of dynamin disassembly (Figure 4A). Upon addition of GTP, we detected a rapid, transient increase in BODIPY self-quenching that was immediately reversed by a relatively slow dequenching reaction. We interpret the initial decrease in emission intensity to reflect a transient conformational rearrangement triggered by GTP binding, similar to that seen and stabilized by GMPPCP. Subsequent GTP hydrolysis appears to elicit a major conformational change in membrane-bound, self-assembled dynamin that triggers its disassembly.

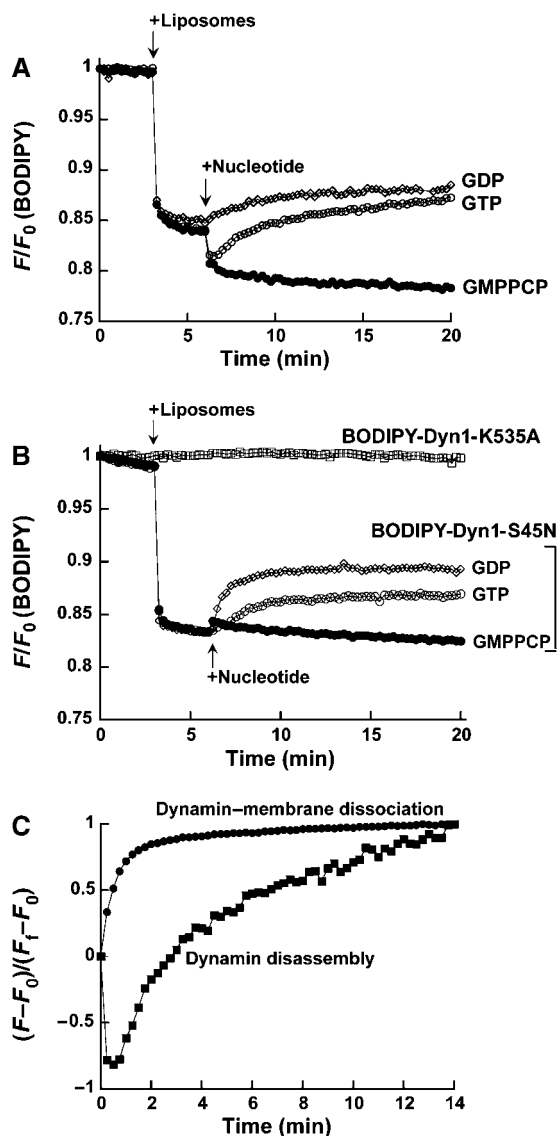


**Figure 4** GTP hydrolysis triggers a major conformational rearrangement in membrane-associated dynamin. (A) Representative time-dependent emission-intensity profiles for 0.1 μM BODIPY-dynamin upon sequential additions of 15 mol% PIP<sub>2</sub>-containing liposomes (30 μM total lipid) at 3 min and the indicated nucleotides (1 mM final) at 6 min. (B) Same as in (A) except using 0.1 μM of either the lipid binding-defective BODIPY-DynK535A (only liposomes were added) or BODIPY-Dyn1S45N, a dynamin mutant defective in GTP binding. (C) Direct comparison of the rate of dynamin-membrane dissociation and the rate of dynamin disassembly. Profiles for NBD emission-intensity decrease (dynamin-membrane dissociation; Figure 3A) and BODIPY emission-intensity increase (dynamin disassembly; (A)) upon addition of 1 mM GTP were normalized and plotted as the total fractional intensity change as a function of time as in Figure 2C. Rate constants for dynamin-membrane dissociation and dynamin disassembly were determined as described in Supplementary data.

We tested this interpretation using a mutant dynamin, BODIPY-labeled Dyn1-S45N, that can bind GDP but not GTP (Damke *et al.*, 2001). As expected, addition of GMPPCP to pre-assembled BODIPY-labeled Dyn1-S45N (BODIPY-Dyn1S45N) did not elicit any further BODIPY self-quenching (Figure 4B), whereas GDP addition triggered the rapid disassembly of BODIPY-Dyn1S45N from the membrane surface. In contrast to the effects on BODIPY-labeled WT-dynamin,

addition of GTP failed to elicit a transient increase in BODIPY self-quenching. Instead, we observed a slow rate of BODIPY dequenching, attributable to the small fraction of GDP contaminating our GTP samples.

A comparison of the rate of change of NBD and BODIPY emission intensity in pre-assembled dynamin upon addition of GTP revealed that dynamin disassembly was significantly slower ( $k = 1.0 \pm 0.1 \text{ min}^{-1}$ ) than dynamin-membrane dissociation ( $k = 2.2 \pm 0.1 \text{ min}^{-1}$ ). This temporal relationship indicates that dynamin dissociates from the membrane as partial assemblies rather than as individual subunits and suggests that dynamin-membrane dissociation is not a direct consequence of a loss of avidity but rather reflects a conformational change that reduces dynamin's affinity for the membrane. Unexpectedly, there was no lag in membrane dissociation during the initial GTP hydrolysis-dependent conformational rearrangement that precedes dynamin disassembly (Figure 4B). This suggests that, as has been observed by others (Danino *et al.*, 2004), after a concerted conformational rearrangement, dynamin dissociates from the ends of assembled spirals very rapidly, whereas the internal rungs of a spiral retain the GTP-dependent conformation and disassemble more slowly.

#### SNX9 and AmphI differentially affect dynamin-membrane interactions

How might this putative nucleotide-dependent, mechanochemical conformational change be coupled to the underlying membrane to accomplish fission? During clathrin-mediated endocytosis, dynamin interacts and functions in concert with numerous SH3 domain-containing proteins, including major binding partners, sorting nexin 9 (SNX9) and amphiphysin I (AmphI) (David *et al.*, 1996; Takei *et al.*, 1999; Lundmark and Carlsson, 2004; Soulet *et al.*, 2005). SNX9 and AmphI both bind clathrin and AP-2 and have been implicated in the targeted recruitment of dynamin to coated pits at the plasma membrane (McMahon *et al.*, 1997; Slepnev *et al.*, 2000; Soulet *et al.*, 2005). Both possess a lipid-binding, triple-helical BAR (Bin/amphiphysin/Rvs) domain that may sense membrane curvature (Peter *et al.*, 2004). In addition, SNX9 contains a phox homology (PX) domain that specifically binds to membrane phosphoinositides (Pylypenko *et al.*, 2007; Yarar *et al.*, 2007). *In vitro* studies have suggested that SNX9 enhances both dynamin's basal and stimulated GTPase activities by promoting its self-assembly in solution and onto liposomes, respectively (Soulet *et al.*, 2005). Results with AmphI have been more ambiguous. AmphI has been shown to either inhibit or stimulate dynamin's GTPase activity depending on bilayer curvature (Yoshida *et al.*, 2004; Soulet *et al.*, 2005). It has also been shown in EM studies to couple dynamin assembly to clathrin lattices and, in light scattering studies, to enhance dynamin-dependent fission of model liposomes (Takei *et al.*, 1999).

We first explored the effects of SNX9 on dynamin-membrane interactions. Addition of an equimolar amount of SNX9 to NBD-dynamin pre-incubated with PIP<sub>2</sub>-containing liposomes under subsaturating conditions resulted in an increase in the recruitment of dynamin to the membrane reaching near-saturable levels (Figure 5A, open circles). In the alternate order, addition of PIP<sub>2</sub>-containing liposomes to an equimolar mixture of SNX9 and NBD-dynamin again resulted

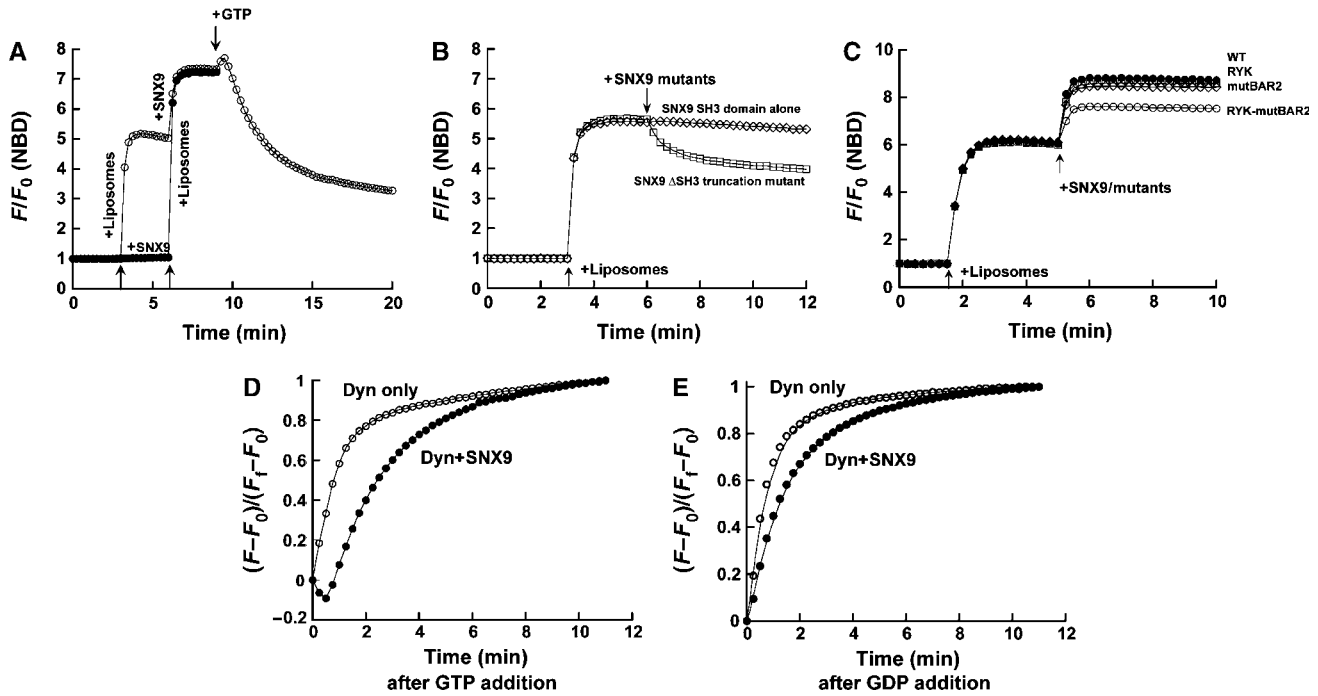


**Figure 5** SNX9 stabilizes dynamin–membrane interactions. (A) Representative time-dependent emission-intensity profiles for 0.05  $\mu\text{M}$  NBD-dynamin before and after sequential additions (arrows) of 15 mol%  $\text{PIP}_2$ -containing liposomes (15  $\mu\text{M}$  total lipid) and 0.05  $\mu\text{M}$  SNX9 ( $\circ$ ) or vice versa ( $\bullet$ ), and upon addition of GTP (1 mM final; arrow). (B) SNX9 SH3 domain is necessary but not sufficient for enhanced dynamin–membrane recruitment. Experiments were performed as in (A), except using the SNX9 SH3 domain alone or the SNX9 $\Delta\text{SH3}$  truncation mutant as indicated. (C) Both PX and BAR domains are required for SNX9-mediated stabilization of dynamin–membrane interactions. Same as in (A) except that SNX9 mutants defective either in PX domain (RYK;  $\square$ ) or BAR domain (mutBAR2;  $\diamond$ ) functions or both (RYK-mutBAR2;  $\circ$ ) as described by Yarar *et al* (2007) were used and compared to WT SNX9 ( $\bullet$ ). For these experiments, 0.4  $\mu\text{m}$  diameter liposomes containing 62.5 mol% DOPC, 15 mol% DOPE, 15 mol% DOPS and 7.5 mol%  $\text{PIP}_2$  were used. (D, E). To directly compare the rates of dynamin–membrane dissociation upon addition of either GTP (D) or GDP (E) in the presence or absence of SNX9, each intensity profile was normalized and plotted as the total fractional intensity change as a function of time as in Figure 2C. Rate constants for dissociation in the presence of GTP (D) or GDP (E) in the presence or absence of SNX9 were determined as described under Supplementary data.

in the enhanced recruitment of NBD-dynamin to the membrane (Figure 5A, closed circles).

Neither the SNX9- $\Delta\text{SH3}$  truncation mutant nor the SNX9-SH3 domain alone enhanced dynamin membrane recruitment (Figure 5B). Indeed, SNX9- $\Delta\text{SH3}$  competed with NBD-dynamin for membrane binding even at vast membrane excess (protein-to-lipid ratio of 1:150). Thus, both SNX9 SH3 domain-dynamin PRD interactions and the SNX9 BAR/PX domains are required to enhance dynamin self-assembly and membrane binding. To further explore the contributions of the PX and BAR domains to this activity, we tested SNX9 PX-domain (RYK mutant) or BAR-domain (mutBAR2) mutants defective in SNX9–liposome interactions (Yarar *et al*, 2007). Whereas either mutant alone did not appreciably affect SNX9’s ability to stabilize dynamin–membrane interactions (Figure 5C), the double mutant defective in both PX and BAR-domain functions (RYK-mutBAR2 mutant) exhibited significant impairment in this activity (Figure 5C). These data, taken together, indicated that SNX9 synergistically enhances dynamin recruitment onto a target membrane surface via cooperative PH/PX/BAR domain–membrane interactions and also by promoting dynamin self-assembly.

We next examined whether SNX9 could stabilize dynamin–membrane interactions during GTP hydrolysis. The presence of equimolar SNX9 transiently stabilized pre-assembled NBD-dynamin on liposomes following addition of GTP, resulting in a detectable lag ( $\sim 30$  s) that preceded GTP

hydrolysis-triggered dynamin–membrane dissociation (Figure 5A and D). Moreover, in the presence of SNX9, the rate of dynamin–membrane dissociation at the onset of stimulated GTP hydrolysis was slower ( $k = 0.4 \pm 0.1 \text{ min}^{-1}$ ) than that of dynamin by itself ( $k = 1.3 \pm 0.3 \text{ min}^{-1}$ ) (Figure 5D). The lag preceding dynamin–membrane dissociation in the presence of SNX9 was specific for GTP and not GDP (Figure 5E), suggesting that SNX9 preferentially stabilizes dynamin on the membrane in the GTP-bound state, while also simultaneously stimulating dynamin’s assembly-dependent GTPase activity (Soulet *et al*, 2005). In this way, SNX9 could localize and couple dynamin’s putative GTP hydrolysis-dependent mechanochemical conformational changes to the underlying membrane.

In stark contrast to SNX9, addition of an equimolar amount of Amphi to pre-assembled NBD-dynamin on  $\text{PIP}_2$ -containing liposomes resulted in the rapid dissociation of dynamin before a new steady state was obtained (Figure 6). A similar lower steady state was obtained when liposomes were added to an equimolar mixture of Amphi and NBD-dynamin pre-incubated in solution (Figure 6). Subsequent addition of GTP resulted in the further dissociation of dynamin from the membrane surface, reaching a new, very low steady state of dynamin–membrane binding (Figure 6). Thus, despite their structural similarity, SNX9 and Amphi either stabilize or destabilize dynamin–membrane interactions, respectively. Together, these data emphasize the specificity of SNX9 in

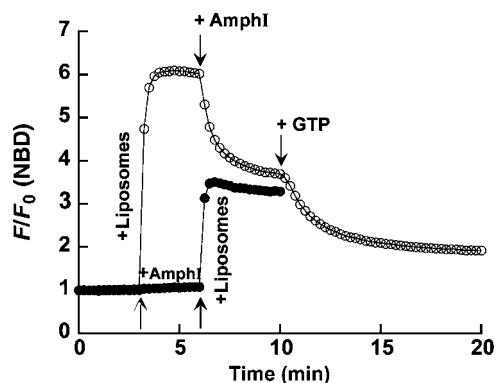


**Figure 6** Amphiphysin destabilizes dynamin–membrane interactions. Representative time-dependent emission-intensity profiles for 0.05  $\mu\text{M}$  NBD-dynamin before and after sequential additions of 15 mol% PIP<sub>2</sub>-containing liposomes (15  $\mu\text{M}$  total lipid) and 0.05  $\mu\text{M}$  Amphi (○) or vice versa (●), and upon addition of GTP (1 mM final).

coupling dynamin's mechanochemical activities to the membrane.

## Discussion

We have developed and employed new fluorescence spectroscopic assays that monitor dynamin–membrane and dynamin–dynamin interactions in real time, providing good temporal resolution and a sensitivity level amenable for simple quantitative measurements. Our results provide several new insights into dynamin function and into how cycles of GTP binding and hydrolysis might be coupled to membrane destabilization and fission. Specifically, we show that (1) dynamin interacts stably with PIP<sub>2</sub>-containing membranes by inserting partially into the lipid bilayer, (2) association of dynamin with these membranes is highly dependent on PIP<sub>2</sub> spatial density, (3) dynamin interacts preferentially with highly curved membranes consistent with its mechanochemical role at the necks of deeply invaginated coated pits *in vivo*, (4) dynamin exhibits a higher affinity for the target membrane in the GTP-bound state than in the GDP-bound state; the switch from a GTP-bound to a GDP-bound conformation upon GTP hydrolysis appears to determine dynamin–membrane association and dissociation, respectively, (5) dynamin–membrane dissociation occurs faster than dynamin disassembly, suggesting that dynamin dissociates from the membrane as partial assemblies rather than as completely unassembled subunits, (6) GTP hydrolysis elicits a major conformational rearrangement in self-assembled dynamin that immediately precedes its disassembly, and (7) whereas SNX9 transiently stabilizes dynamin–membrane association, presumably localizing dynamin's mechanochemical conformational rearrangements to the underlying membrane, Amphi has the opposite effect.

Multiple lines of evidence suggest that dynamin functions at both early and late stages of endocytosis (Narayanan *et al.*, 2005; Macia *et al.*, 2006). Indeed, most dominant-negative mutants of dynamin, including RCL-Dyn<sup>I533C</sup>, block early, rate-limiting stages of clathrin-mediated endocytosis before dynamin self-assembly and the formation of constricted coated pits (Damke *et al.*, 2001). Herein, we focus exclusively on dynamin activities (lipid binding, self-assembly,

assembly-stimulated GTPase activity and dynamin–effector interactions) required for late events in endocytosis. For each of these activities, NBD-dynamin (RCL-Dyn<sup>I533C-NBD</sup>) and BODIPY-dynamin are demonstrably equivalent to unlabeled WT-dynamin and to each other. Moreover, both NBD- and BODIPY-dynamins are similarly regulated by guanine nucleotides, and the differential effects of SNX9 and Amphi on NBD-dynamin–membrane interactions are consistent with their effects on WT-dynamin self-assembly and assembly-stimulated GTPase activities (Owen *et al.*, 1998; Soulet *et al.*, 2005). Therefore, although there are clearly other aspects of dynamin function required for clathrin-mediated endocytosis *in vivo*, these dynamin derivatives appear to retain and faithfully report the membrane-associated mechanochemical properties of dynamin studied here.

Previous studies that examined dynamin association with lipid monolayers had suggested that dynamin is a membrane-active molecule capable of inserting a large surface area into the acyl chain region of a membrane monolayer (Burger *et al.*, 2000). Using spin-labeled lipids and collisional quenching of fluorescence, we have identified the relatively hydrophobic VL1 of the PH domain of dynamin, previously implicated in PIP<sub>2</sub> headgroup recognition, as one region of dynamin that inserts partially into the hydrophobic core of a membrane bilayer. Thus, similar to the N-terminal amphipathic helix of Arf family GTPases that insert partially into one leaflet of a bilayer (Antonny, 2006), the PH domains of a self-assembled dynamin polymer may act as ‘wedges’ or ‘footprints’ that asymmetrically expand one leaflet of a membrane bilayer against the other, ultimately bending the membrane.

The sensitivity of dynamin–membrane interactions to PIP<sub>2</sub> concentration and the sigmoidal dependence of this interaction on PIP<sub>2</sub> spatial density possibly reflects a ‘reduction of dimensionality effect’ (Mosior and McLaughlin, 1992) in which the low-affinity binding of a single PH domain in a dynamin tetramer to the first PIP<sub>2</sub> molecule increases the proximity of the rest of the PH domains to nearby PIP<sub>2</sub> molecules, leading to cooperative, high-avidity membrane association. Similar mechanisms have been described for the N-WASP B-motif and the MARCKS peptide (Wang *et al.*, 2001; Papayannopoulos *et al.*, 2005). Significant association of dynamin only with liposomes that contain  $\geq 5$  mol% PIP<sub>2</sub>, under our *in vitro* conditions, also suggests that high local concentrations of PIP<sub>2</sub> generated during clathrin-mediated endocytosis may play a role in dynamin stabilization *in vivo*.

Dynamin preferentially associated with more highly curved membranes *in vitro*, consistent with previous studies that have demonstrated a higher assembly-stimulated GTPase activity for dynamin on small versus large liposomes (Yoshida *et al.*, 2004). Collectively, these data suggest that dynamin must overcome a larger thermodynamic barrier in bending and deforming the relatively flatter membrane of a large liposome for efficient self-assembly when compared to smaller liposomes with higher intrinsic curvature. In the physiological context, generation of highly curved coated pit necks by polymerizing clathrin lattices and accessory molecules (Ford *et al.*, 2002) may overcome this energy barrier required for efficient dynamin self-assembly. Consistent with this notion, the burst of dynamin self-assembly observed at endocytic sites by TIRF microscopy (Merrifield *et al.*, 2002) may reflect a preferential redistribution of dynamin, initially recruited to the clathrin lattice

through SH3 domain interactions, to sites of high lipid curvature, that is, coated pit necks, during the late stages of coated vesicle formation.

The differential effects of GMPPCP, GTP and GDP on dynamin–membrane interactions indicate that, during GTP binding and hydrolysis, dynamin cycles through distinct conformations that progressively strengthen and weaken its interaction with the membrane. The weakened dynamin–membrane interactions of the GDP-bound versus the nucleotide-free state suggests that GDP-dependent conformational changes in the GTPase domain, however minor (Niemann *et al*, 2001), are amplified and relayed to the PH domain to effect dynamin–membrane dissociation. Thus, our data suggest that the dynamin GTPase and PH domains, although spatially separated, are conformationally coupled. Consistent with this, fluorescence studies of dynamin in solution have detected nucleotide-dependent changes in PH domain conformation using intrinsic Trp emission intensity (Solomaha and Palfrey, 2005). Atomic resolution structures of full-length dynamin under various nucleotide-bound states will be required to elucidate the molecular mechanisms underlying this long-range conformational relay.

Our kinetic experiments with NBD- and BODIPY-labeled dynamins demonstrate that GTP hydrolysis elicits a major conformational rearrangement in self-assembled dynamin, before triggering disassembly. Here, we show that SNX9, a major dynamin binding partner (Lundmark and Carlsson, 2004; Soulet *et al*, 2005), stabilizes membrane-associated dynamin during stimulated GTP hydrolysis (Soulet *et al*, 2005). Thus, SNX9 may function as a downstream effector that helps transduce the free energy of dynamin GTP hydrolysis toward membrane destabilization events that are required for fission.

Takei *et al* (1999) reported a progressive reduction in the light scattering of dynamin-coated liposomes upon sequential addition of AmphI and GTP and suggested that AmphI enhances GTP-dependent fragmentation of dynamin-coated liposomes. However, our fluorescence-based data demonstrating dynamin–membrane dissociation upon sequential additions of AmphI and GTP suggest an alternate interpretation: that the observed changes in light scattering, in part, reflect protein dissociation from the membrane.

Taken together, our dynamic measurements of dynamin–membrane and dynamin–dynamin interactions suggest that the mechanism(s) of dynamin-mediated membrane fission involve a combination of partial membrane penetration, membrane tubule constriction and stabilization of GTP-dependent mechanochemical conformational changes on the membrane by effectors that regulate dynamin function. We propose that transient bilayer destabilization as a result of these conformational changes and the rapid dissociation of self-assembled dynamin from the membrane upon GTP hydrolysis may ultimately trigger membrane fission.

## Materials and methods

### Preparation of RCL-Dyn<sup>I533C</sup>

cDNA encoding human WT-Dyn1 subcloned in pBluescript II KS+ (Stratagene) was used as the template for PCR-based mutagenesis using the Quikchange method (Stratagene). All mutations were confirmed by automated DNA sequencing. The BamHI–StuI fragment carrying the I533C mutation, along with Cys to Ser substitutions at residue positions 86, 424, 427, 442 and 607, was

then used to replace the corresponding fragment of Cys-less-Dyn1 cDNA subcloned previously in pVL1393 (AB Vector). Recombinant baculoviruses harboring this cDNA construct were generated, and RCL-Dyn<sup>I533C</sup> was expressed in infected Tn5 insect cells, purified and stored as described previously (Leonard *et al*, 2005; Ramachandran *et al*, 2007), except that no DTT and only 10% (v/v) glycerol was used in the storage buffer. Protein concentration was determined by absorbance at 280 nm using a molar absorptivity coefficient ( $\epsilon_{280}$ ) of  $58\,790\text{ M}^{-1}\text{ cm}^{-1}$ .

### Preparation of AmphI and SNX9

GST-tagged human amphiphysin I (GST-AmphI) (gift of Pietro De Camilli, Yale University) was expressed in *Escherichia coli* BL21 (DE3) and purified using glutathione–sepharose according to standard procedures. SNX9 and SNX9 mutants were prepared as described previously (Soulet *et al*, 2005; Yasar *et al*, 2007).

### Preparation of NBD- and BODIPY-dynamins

Cys at position 533 in RCL-Dyn<sup>I533C</sup> was selectively labeled in the absence of reducing agent with NBD using *N,N'*-dimethyl-*N*-(iodoacetyl)-*N'*-(7-nitrobenz-2-oxa-1,3-diazol-4-yl)ethylenediamine (Invitrogen) dissolved in DMSO, which was added at an equimolar ratio (to avoid modification of the partially buried native Cys at position 169) to about  $15\text{ }\mu\text{M}$  of RCL-Dyn<sup>I533C</sup> in a final reaction volume of  $500\text{ }\mu\text{l}$ . After 1 h at room temperature, DTT was added to  $5\text{ mM}$  to stop the reaction. The mixture was then extensively dialyzed against buffer containing  $20\text{ mM}$  HEPES, pH 7.5,  $150\text{ mM}$  KCl and  $1\text{ mM}$  DTT to separate NBD-dynamin from the dye-DTT adduct. After high-speed ultracentrifugation ( $100\,000\text{ g}$ ) to discard any precipitated protein, the efficiency of labeling was determined to be 30–60% using a molar absorptivity coefficient of  $25\,000\text{ M}^{-1}\text{ cm}^{-1}$  at  $478\text{ nm}$  for NBD. NBD-dynamin was stored on ice and used within a week of production. NBD-labeling of Dyn-RCL<sup>S306C</sup> was performed and purified using similar procedures.

For BODIPY-labeled dynamin derivatives, Dyn1-WT, Dyn1-S45N or Dyn1-K535A was labeled with a tenfold molar excess of the thiol-reactive iodoacetamide derivative of BODIPY-Fl (Invitrogen) and purified as described earlier (Ramachandran *et al*, 2007). The efficiency of labeling was determined using molar absorptivity coefficients of  $58\,790\text{ M}^{-1}\text{ cm}^{-1}$  at  $280\text{ nm}$  and  $76\,000\text{ M}^{-1}\text{ cm}^{-1}$  at  $502\text{ nm}$  for dynamin and BODIPY, respectively. The typical labeling efficiency was 1:1 (one mole of BODIPY per mole of dynamin). Self-quenching of BODIPY dyes occurs by the formation of non-fluorescent, ground-state dark dimers and homo-FRET from neighboring, unquenched BODIPY molecules (Bergstrom *et al*, 2002).

### Preparation of liposomes

All phospholipids were purchased from Avanti Polar Lipids Inc. Liposomes were generated according to procedures described previously (Ramachandran *et al*, 2007). Unless otherwise stated,  $0.1\text{ }\mu\text{m}$  diameter liposomes were used. Briefly, liposomes containing either 100 mol% 1,2-dioleoyl-*sn*-glycero-3-phosphocholine (DOPC; Avanti polar lipids) or a mixture of DOPC and porcine PIP<sub>2</sub> at the different mole percentages (mol%) indicated were prepared by extrusion through polycarbonate membranes of varying pore diameters as mentioned. Liposomes used in lipophilic quenching experiments were prepared using DOPC and PIP<sub>2</sub> (15 mol%) in the same way, except that 10 mol% of the DOPC was replaced by a nitroxide-labeled phospholipid, either 1-palmitoyl-2-stearoyl-(*x*-doxyl)-*sn*-glycero-3-phospholipid (*x* is equal to 5 or 12 and refers to the carbon position in the acyl chain to which the quencher moiety is attached) or 1,2-dioleoyl-*sn*-glycero-3-phosphotempochole (where the nitroxide is positioned on the phospholipid headgroup).

### Fluorescence spectroscopy

Unless otherwise indicated, all intensity measurements shown were carried out with  $0.1\text{ }\mu\text{M}$  NBD- or BODIPY-dynamin in buffer containing  $20\text{ mM}$  HEPES, pH 7.5,  $150\text{ mM}$  KCl and  $1\text{ mM}$  MgCl<sub>2</sub> at  $25^\circ\text{C}$  using the instrumentation described earlier (Ramachandran *et al*, 2007). Increasing Mg<sup>2+</sup> concentration in the buffer resulted in the reduced initial binding of dynamin to PIP<sub>2</sub>-containing liposomes (Toner *et al*, 1988). For the sub-saturable binding of dynamin to PIP<sub>2</sub>-containing liposomes in experiments that included SNX9 and AmphI,  $0.05\text{ }\mu\text{M}$  dynamin and  $2\text{ mM}$  MgCl<sub>2</sub> final concentrations were used. In experiments performed with the GTP regenerating

system, the final MgCl<sub>2</sub> concentration was 5 mM (Ingerman *et al.*, 2005; Ramachandran *et al.*, 2007). The final nucleotide concentration in all relevant experiments was 1 mM.

For time-dependent emission intensity and spectral measurements (2.4 ml final volume) 1 cm × 1 cm quartz cuvettes were used, whereas for end-point measurements (260 μl final volume) 4 mm × 4 mm quartz cuvettes were used. For the acquisition of NBD emission spectra, the dye was excited at 470 nm (4-nm bandpass) and emission intensity was measured between 500 and 600 nm (4-nm bandpass). For end-point measurements, NBD-dynamin was excited at 470 nm (4-nm bandpass) and emission intensity was measured at 530 nm (4-nm bandpass) to establish  $F_0$ . Liposomes were then added to these samples and incubated for 10 min to allow saturable binding before the final intensity value,  $F$ , was measured. For the acquisition of time-dependent emission-intensity profiles, samples containing either NBD-dynamin or BODIPY-dynamin were continuously stirred and temperature-equilibrated before and during data acquisition. Data collection was begun and recorded at 15 s intervals (5 s signal integration). NBD was excited at 470 nm (4-nm bandpass) and emission was monitored at 530 nm (4-nm bandpass). BODIPY was excited at 490 nm (2-nm bandpass) and emission was monitored at 510 nm (2-nm bandpass). After the initial intensity baseline was obtained, at the time points indicated, either nucleotide (1 mM final) or PIP<sub>2</sub>-containing liposomes (1:300 molar ratio of protein to lipid) were added to the sample. To obtain rate constants, data were fit using

## References

- Achiriloaie M, Barylko B, Albanesi JP (1999) Essential role of the dynamin pleckstrin homology domain in receptor-mediated endocytosis. *Mol Cell Biol* **19**: 1410–1415
- Antony B (2006) Membrane deformation by protein coats. *Curr Opin Cell Biol* **18**: 386–394
- Artalejo CR, Lemmon MA, Schlessinger J, Palfrey HC (1997) Specific role for the PH domain of dynamin-1 in the regulation of rapid endocytosis in adrenal chromaffin cells. *EMBO J* **16**: 1565–1574
- Bergstrom F, Mikhalyov I, Hagglof P, Wortmann R, Ny T, Johansson LB (2002) Dimers of dipyrrometheneboron difluoride (BODIPY) with light spectroscopic applications in chemistry and biology. *J Am Chem Soc* **124**: 196–204
- Binns DD, Barylko B, Grichine N, Atkinson MA, Helms MK, Jameson DM, Eccleston JF, Albanesi JP (1999) Correlation between self-association modes and GTPase activation of dynamin. *J Protein Chem* **18**: 277–290
- Burger KN, Demel RA, Schmid SL, de Kruijff B (2000) Dynamin is membrane-active: lipid insertion is induced by phosphoinositides and phosphatidic acid. *Biochemistry* **39**: 12485–12493
- Chen YJ, Zhang P, Egelman EH, Hinshaw JE (2004) The stalk region of dynamin drives the constriction of dynamin tubes. *Nat Struct Mol Biol* **11**: 574–575
- Conner SD, Schmid SL (2003) Regulated portals of entry into the cell. *Nature* **422**: 37–44
- Damke H, Binns DD, Ueda H, Schmid SL, Baba T (2001) Dynamin GTPase domain mutants block endocytic vesicle formation at morphologically distinct stages. *Mol Biol Cell* **12**: 2578–2589
- Danino D, Moon KH, Hinshaw JE (2004) Rapid constriction of lipid bilayers by the mechanochemical enzyme dynamin. *J Struct Biol* **147**: 259–267
- David C, McPherson PS, Mundigl O, de Camilli P (1996) A role of amphiphysin in synaptic vesicle endocytosis suggested by its binding to dynamin in nerve terminals. *Proc Natl Acad Sci USA* **93**: 331–335
- Ford MG, Mills IG, Peter BJ, Vallis Y, Praefcke GJ, Evans PR, McMahon HT (2002) Curvature of clathrin-coated pits driven by epsin. *Nature* **419**: 361–366
- Hinshaw JE (2000) Dynamin and its role in membrane fission. *Annu Rev Cell Dev Biol* **16**: 483–519
- Ingerman E, Perkins EM, Marino M, Mears JA, McCaffery JM, Hinshaw JE, Nunnari J (2005) Dnm1 forms spirals that are structurally tailored to fit mitochondria. *J Cell Biol* **170**: 1021–1027
- Johnson AE (2005) Fluorescence approaches for determining protein conformations, interactions and mechanisms at membranes. *Traffic* **6**: 1078–1092
- Lee A, Frank DW, Marks MS, Lemmon MA (1999) Dominant-negative inhibition of receptor-mediated endocytosis by a dynamin-1 mutant with a defective pleckstrin homology domain. *Curr Biol* **9**: 261–264
- Leonard M, Song BD, Ramachandran R, Schmid SL (2005) Robust colorimetric assays for dynamin's basal and stimulated GTPase activities. *Methods Enzymol* **404**: 490–503
- Lundmark R, Carlsson SR (2004) Regulated membrane recruitment of dynamin-2 mediated by sorting nexin 9. *J Biol Chem* **279**: 42694–42702
- Macia E, Ehrlich M, Massol T, Boucrot E, Brunner C, Kirchhausen T (2006) Dynasore, a cell permeable inhibitor of dynamin. *Dev Cell* **10**: 839–850
- McMahon HT, Gallop JL (2005) Membrane curvature and mechanisms of dynamic cell membrane remodelling. *Nature* **438**: 590–596
- McMahon HT, Wigge P, Smith C (1997) Clathrin interacts specifically with amphiphysin and is displaced by dynamin. *FEBS Lett* **413**: 319–322
- Merrifield CJ, Feldman ME, Wan L, Almers W (2002) Imaging actin and dynamin recruitment during invagination of single clathrin-coated pits. *Nat Cell Biol* **4**: 691–698
- Mosior M, McLaughlin S (1992) Electrostatics and reduction of dimensionality produce apparent cooperativity when basic peptides bind to acidic lipids in membranes. *Biochim Biophys Acta* **1105**: 185–187
- Narayanan R, Leonard M, Song BD, Schmid SL, Ramaswami M (2005) An internal GAP domain negatively regulates presynaptic dynamin *in vivo*: a two-step model for dynamin function. *J Cell Biol* **169**: 117–126
- Niemann HH, Knetsch ML, Scherer A, Manstein DJ, Kull FJ (2001) Crystal structure of a dynamin GTPase domain in both nucleotide-free and GDP-bound forms. *EMBO J* **20**: 5813–5821
- Okamoto PM, Herskovits JS, Vallee RB (1997) Role of the basic, proline-rich region of dynamin in Src homology 3 domain binding and endocytosis. *J Biol Chem* **272**: 11629–11635
- Owen DJ, Wigge P, Vallis Y, Moore JD, Evans PR, McMahon HT (1998) Crystal structure of the amphiphysin-2 SH3 domain and its role in the prevention of dynamin ring formation. *EMBO J* **17**: 5273–5285
- Papayannopoulos V, Co C, Prehoda KE, Snapper S, Taunton J, Lim WA (2005) A polybasic motif allows N-WASP to act as a sensor of PIP(2) density. *Mol Cell* **17**: 181–191
- Peter BJ, Kent HM, Mills IG, Vallis Y, Butler PJ, Evans PR, McMahon HT (2004) BAR domains as sensors of membrane curvature: the amphiphysin BAR structure. *Science* **303**: 495–499

either Kaleidagraph or Graphpad prism data analysis software as described in Supplementary data.

### GTPase and sedimentation assays

All nucleotides were purchased from Sigma Inc. Basal and assembly-stimulated GTP hydrolysis rates of NBD-, BODIPY- and WT-dynamins were monitored as a function of time using a malachite green-based colorimetric assay as described previously (Leonard *et al.*, 2005). Dynamin was separated into liposome-bound (pellet, P) and soluble (supernatant, S) fractions by high-speed centrifugation also as described earlier (Ramachandran *et al.*, 2007).

### Supplementary data

Supplementary data are available at *The EMBO Journal* Online (<http://www.embojournal.org>).

## Acknowledgements

We thank Quint Le Duc for early experiments, Drs Mark Surka and Defne Yazar for providing SNX9, Sharmista Acharya, Vasily Lukiyanchuk and Marilyn Leonard for excellent technical assistance and Schmid lab members for critical comments. This work was supported by NIH Grants R01.GM42455 and R37.MH61345 to SLS and an American Heart Association postdoctoral fellowship (AHA 0625090Y) to RR. This is TSRI manuscript no. 19086.

- Pylypenko O, Lundmark R, Rasmuson E, Carlsson SR, Rak A (2007) The PX-BAR membrane-remodeling unit of sorting nexin 9. *EMBO J* **26**: 4788–4800
- Ramachandran R, Heuck AP, Tweten RK, Johnson AE (2002) Structural insights into the membrane-anchoring mechanism of a cholesterol-dependent cytolysin. *Nat Struct Biol* **9**: 823–827
- Ramachandran R, Surka M, Chappie JS, Fowler DM, Foss TR, Song BD, Schmid SL (2007) The dynamin middle domain is critical for tetramerization and higher-order self-assembly. *EMBO J* **26**: 559–566
- Ramachandran R, Tweten RK, Johnson AE (2004) Membrane-dependent conformational changes initiate cholesterol-dependent cytolysin oligomerization and intersubunit beta-strand alignment. *Nat Struct Mol Biol* **11**: 697–705
- Ramachandran R, Tweten RK, Johnson AE (2005) The domains of a cholesterol-dependent cytolysin undergo a major FRET-detected rearrangement during pore formation. *Proc Natl Acad Sci USA* **102**: 7139–7144
- Roux A, Uyhazi K, Frost A, De Camilli P (2006) GTP-dependent twisting of dynamin implicates constriction and tension in membrane fission. *Nature* **441**: 528–531
- Salim K, Bottomley MJ, Querfurth E, Zvelebil MJ, Gout I, Scaife R, Margolis RL, Gigg R, Smith CI, Driscoll PC, Waterfield MD, Panayotou G (1996) Distinct specificity in the recognition of phosphoinositides by the pleckstrin homology domains of dynamin and Bruton's tyrosine kinase. *EMBO J* **15**: 6241–6250
- Sever S, Muhlberg AB, Schmid SL (1999) Impairment of dynamin's GAP domain stimulates receptor-mediated endocytosis. *Nature* **398**: 481–486
- Shatarsky O, Heuck AP, Shepard LA, Rossjohn J, Parker MW, Johnson AE, Tweten RK (1999) The mechanism of membrane insertion for a cholesterol-dependent cytolysin: a novel paradigm for pore-forming toxins. *Cell* **99**: 293–299
- Shpetner HS, Herskovits JS, Vallee RB (1996) A binding site for SH3 domains targets dynamin to coated pits. *J Biol Chem* **271**: 13–16
- Slepnev VI, Ochoa GC, Butler MH, De Camilli P (2000) Tandem arrangement of the clathrin and AP-2 binding domains in amphiphysin 1 and disruption of clathrin coat function by amphiphysin fragments comprising these sites. *J Biol Chem* **275**: 17583–17589
- Solomaha E, Palfrey HC (2005) Conformational changes in dynamin on GTP binding and oligomerization reported by intrinsic and extrinsic fluorescence. *Biochem J* **391**: 601–611
- Song BD, Yasar D, Schmid SL (2004) An assembly-incompetent mutant establishes a requirement for dynamin self-assembly in clathrin-mediated endocytosis *in vivo*. *Mol Biol Cell* **15**: 2243–2252
- Soulet F, Yasar D, Leonard M, Schmid SL (2005) SNX9 regulates dynamin assembly and is required for efficient clathrin-mediated endocytosis. *Mol Biol Cell* **16**: 1058–2067
- Stowell MH, Marks B, Wigge P, McMahon HT (1999) Nucleotide-dependent conformational changes in dynamin: evidence for a mechanochemical molecular spring. *Nat Cell Biol* **1**: 27–32
- Sweitzer SM, Hinshaw JE (1998) Dynamin undergoes a GTP-dependent conformational change causing vesiculation. *Cell* **93**: 1021–1029
- Takei K, Slepnev VI, Haucke V, De Camilli P (1999) Functional partnership between amphiphysin and dynamin in clathrin-mediated endocytosis. *Nat Cell Biol* **1**: 33–39
- Toner M, Vaio G, McLaughlin A, McLaughlin S (1988) Adsorption of cations to phosphatidylinositol 4,5-bisphosphate. *Biochemistry* **27**: 7435–7443
- Vallis Y, Wigge P, Marks B, Evans PR, McMahon HT (1999) Importance of the pleckstrin homology domain of dynamin in clathrin-mediated endocytosis. *Curr Biol* **9**: 257–260
- Wang G, Moniri NH, Ozawa K, Stamler JS, Daaka Y (2006) Nitric oxide regulates endocytosis by S-nitrosylation of dynamin. *Proc Natl Acad Sci USA* **103**: 1295–1300
- Wang J, Arbuzova A, Hangyas-Mihalyn G, McLaughlin S (2001) The effector domain of myristoylated alanine-rich C kinase substrate binds strongly to phosphatidylinositol 4,5-bisphosphate. *J Biol Chem* **276**: 5012–5019
- Yasar D, Surka MC, Leonard MC, Schmid SL (2007) SNX9 activities are regulated by multiple phosphoinositides through the PX and BAR domains. *Traffic* **8** (e-pub ahead of print; doi:10.1111/j.1600-0854.2007.00675.x)
- Yoshida Y, Kinuta M, Abe T, Liang S, Araki K, Cremona O, Di Paolo G, Moriyama Y, Yasuda T, De Camilli P, Takei K (2004) The stimulatory action of amphiphysin on dynamin function is dependent on lipid bilayer curvature. *EMBO J* **23**: 3483–3491
- Zhang P, Hinshaw JE (2001) Three-dimensional reconstruction of dynamin in the constricted state. *Nat Cell Biol* **3**: 922–926
- Zheng J, Cahill SM, Lemmon MA, Fushman D, Schlessinger J, Cowburn D (1996) Identification of the binding site for acidic phospholipids on the pH domain of dynamin: implications for stimulation of GTPase activity. *J Mol Biol* **255**: 14–21